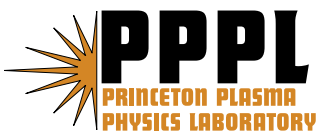# Princeton Plasma Physics Laboratory

Computation of Three Dimensional Tokamak and Spherical Torus Equilibria

Jong-kyu Park, Allen H. Boozer,
and Alan H. Glasser

(Preprint)
May 2007

PPPL
PRINCETON PLASMA
PHYSICS LABORATORY

Princeton Plasma Physics Laboratory
Report Disclaimers

Full Legal Disclaimer

This report was prepared as an account of work sponsored by an agency of the United States Government. Neither the United States Government nor any agency thereof, nor any of their employees, nor any of their contractors, subcontractors or their employees, makes any warranty, express or implied, or assumes any legal liability or responsibility for the accuracy, completeness, or any third party's use or the results of such use of any information, apparatus, product, or process disclosed, or represents that its use would not infringe privately owned rights. Reference herein to any specific commercial product, process, or service by trade name, trademark, manufacturer, or otherwise, does not necessarily constitute or imply its endorsement, recommendation, or favoring by the United States Government or any agency thereof or its contractors or subcontractors. The views and opinions of authors expressed herein do not necessarily state or reflect those of the United States Government or any agency thereof.

Trademark Disclaimer

Reference herein to any specific commercial product, process, or service by trade name, trademark, manufacturer, or otherwise, does not necessarily constitute or imply its endorsement, recommendation, or favoring by the United States Government or any agency thereof or its contractors or subcontractors.

PPPL Report Availability

Princeton Plasma Physics Laboratory:

http://www.pppl.gov/techreports.cfm

Office of Scientific and Technical Information (OSTI):

http://www.osti.gov/bridge

Related Links:

U.S. Department of Energy

Office of Scientific and Technical Information

Fusion Links

Computation of three dimensional tokamak and spherical torus equilibria

Jong-kyu Park,[1, *] Allen H. Boozer,[2] and Alan H. Glasser[3]

[1]*Princeton Plasma Physics Laboratory, Princeton, New Jersey, NJ 08543*
[2]*Department of Applied Physics and Applied Mathematics, Columbia University, New York, NY 10027*
[3]*Los Alamos National Laboratory, Los Alamos, New Mexico, NM 87545*

A nominally axisymmetric plasma configuration, such as a tokamak or a spherical torus, is highly sensitive to non-axisymmetric magnetic perturbations due to currents outside of the plasma. The high sensitivity means that the primary interest is in the response of the plasma to very small perturbations, $\left|\vec{b}/\vec{B}\right| \approx 10^{-2}$ to 10^{-4}, which can be calculated using the theory of perturbed equilibria. The Ideal Perturbed Equilibrium Code (IPEC) is described and applied to the study of the plasma response in a spherical torus to such external perturbations.

I.   INTRODUCTION

Nominally axisymmetric plasma configurations, such the tokamak and the spherical torus, are extremely sensitive to non-axisymmetric magnetic perturbations. This sensitivity implies that the response of axisymmetric equilibria to small non-axisymmetric perturbations is a critical issue in equilibrium design and control [1–5]. The linear response of a plasma equilibrium to a perturbation in which the plasma conserves its safety factor and pressure profile is given by the same equations as the theory of ideal, linear magnetohydrodynamic (MHD) stability [6–8].

The DCON ideal MHD stability code [9] can be used to make calculations of perturbed equilibria, but to do this an interface is required between DCON and the externally produced magnetic fields. This interface is included in the Ideal Perturbed Equilibrium Code (IPEC), which is described in this paper. Many find the method used in IPEC for including external magnetic fields subtle, because it is an inverse method. To aid the physical understanding of the method used in IPEC, a qualitative discussion will be given in the Introduction.

Given an external magnetic perturbation, which can be represented by the normal magnetic field it produces on the unperturbed plasma surface, IPEC finds the resulting displacement of the plasma, $\vec{\xi}(\vec{x})$, and the perturbed magnetic field, $\vec{b}(\vec{x}) = \vec{\nabla} \times (\vec{\xi} \times \vec{B})$ throughout the plasma volume. Some of the applications of this information are also discussed in the Introduction.

A.   Description of IPEC method

To understand the method used by IPEC for including external magnetic fields, consider an ideal MHD axisymmetric equilibrium. The use of DCON to calculate perturbations about this equilibrium gives a set of M plasma displacements $\vec{\xi}_i(\psi, \theta, \varphi)$, which is the set of M

ideal MHD eigenmodes for a given toroidal harmonic number n, where $1 \leq i \leq M$ and M is the number of poloidal harmonics retained in DCON run. Each of these displacements $\vec{\xi}_i$ is associated with a certain deformation of the plasma boundary, $\vec{\xi}_i \cdot \hat{n} \equiv (\vec{\xi}_i \cdot \hat{n})(\psi_b, \theta, \varphi)$, where $\vec{\xi}_i$ is evaluated on the unperturbed plasma boundary at $\psi = \psi_b$ and $\hat{n}$ is the normal to the unperturbed plasma boundary. Each of these M displacements of the plasma boundary $\vec{\xi}_i \cdot \hat{n}$ defines a perturbed equilibrium if an external magnetic field produces a required force to support it. That is, the set of M ideal MHD eigenmodes found by DCON defines a set of M neighboring perturbed equilibria. Each of the neighboring equilibria is supported by an external magnetic field and has the same profiles of pressure and safety factor as the unperturbed equilibrium; only the shape of the plasma has been changed.

To understand that each displacement of the plasma boundary $\vec{\xi}_i \cdot \hat{n}$ is associated with a unique externally produced magnetic field $\vec{b}_i^x$, one can imagine that a thin perfectly-conducting shell surrounds the plasma and is an infinitesimal distance outside. The deformation of the plasma boundary $\vec{\xi}_i \cdot \hat{n}$ is produced by the deformation of the perfectly conducting shell. When the shell is deformed, a current must flow in the shell to make zero normal magnetic field on the shell. Assuming the shell has an infinitesimal thickness, this current is a surface current $\vec{K}_i^x$, which is external to the plasma. The normal component of the externally produced normal magnetic field, $\vec{b}_i^x \cdot \hat{n} \equiv (\vec{b}_i^x \cdot \hat{n})(\psi_b, \theta, \varphi)$, associated with the displacement $\vec{\xi}_i \cdot \hat{n}$ is the normal component of the magnetic field produced by the external surface current $\vec{K}_i^x$. In other words, each of the *actual* magnetic field perturbations calculated by DCON, $\vec{b}_i = \vec{\nabla} \times (\vec{\xi}_i \times \vec{B})$, is the sum of a magnetic field produced by currents within the plasma and an *external* magnetic field $\vec{b}_i^x$ produced by currents outside the plasma, $\vec{K}_i^x$. The actual location and magnitude of the external currents is only relevant to the response of the plasma through their producing an external normal magnetic field $\vec{b}^x \cdot \hat{n}$ at the plasma boundary. This follows from the fact that the magnetic field in the vacuum region between the plasma and the external currents obeys $\vec{b}^x = \vec{\nabla}\chi$ with $\nabla^2 \chi = 0$, and the fact that

Laplace's equation, $\nabla^2 \chi = 0$, has a unique answer that is regular in region bounded by the external currents if the normal component of the external magnetic field is specified on the plasma boundary.

If the perturbed equilibrium is not supported by an external magnetic field, the plasma inertia associated with an eigenfrequency $\omega_i^2 = 2\delta W_i / \int dx^3 \rho |\xi_i|^2$ must supply the required force. The DCON is used for finding perturbed equilibria because it minimizes δW, which gives perturbed equilibria, rather than ω_i. For stable modes, a minimization of ω_i is in effect a maximization of the inertia, so the resulting displacements $\vec{\xi}_i \cdot \hat{n}$ do not represent perturbed equilibria.

Although imagining the plasma is surrounded by a perfectly-conducting shell provides a compelling basis for defining the external magnetic field associated with each plasma perturbation, calculations are easier using a control surface that is located just outside the unperturbed plasma surface, and this is the method used in IPEC. A plasma displacement determines a magnetic perturbation $\vec{b} = \nabla \times (\vec{\xi} \times \vec{B})$, so IPEC uses the displacement of the plasma boundary $\vec{\xi} \cdot \hat{n}$ to determine a part of the perturbed magnetic field that is normal to the unperturbed plasma boundary, $\vec{b} \cdot \hat{n}$, and a part that is tangential to the plasma boundary, $\hat{n} \times \vec{b}^{(p)}$. Since the normal field $\vec{b} \cdot \hat{n}$ is continuous across the plasma boundary and the control surface, $\vec{b} \cdot \hat{n}$ then gives a unique vacuum field outside the plasma, $\vec{b}^{(vo)}$, that vanishes at infinity. The difference between the tangential field infinitesimally outside the control surface $\hat{n} \times \vec{b}^{(vo)}$ and the tangential field on the plasma side of the control surface $\hat{n} \times \vec{b}^{(p)}$ determines an external surface current on the control surface, $\mu_0 \vec{K}^x = \hat{n} \times \vec{b}^{(vo)} - \hat{n} \times \vec{b}^{(p)}$. Once $\vec{K}^x$ is known, the externally produced normal magnetic field $\vec{b}^x \cdot \hat{n}$ can be found by $\nabla \times \vec{b}^x = \mu_0 \vec{j}^x$ in vacuum.

Each of the M neighboring equilibria calculated by DCON has a unique distribution of the external normal magnetic field $\vec{b}_i^x \cdot \hat{n}$, where $1 \leq i \leq M$, that must be produced by currents outside the plasma to sustain that equilibrium. If an external magnetic perturbation, such as that due to a magnetic field error $\vec{b}^x \cdot \hat{n}$, is specified on the unperturbed plasma boundary, this perturbation can be expanded as $\vec{b}^x \cdot \hat{n} = \sum_{i=1}^M c_i \vec{b}_i^x \cdot \hat{n}$, with expansion coefficients c_i. If this is done, the plasma displacement that gives the perturbed equilibrium produced by the field error is $\vec{\xi}(\psi, \theta, \varphi) = \sum_{i=1}^M c_i \vec{\xi}_i(\psi, \theta, \varphi)$. This is the method used by IPEC to find the perturbed equilibrium associated with a given magnetic field error. More information about numerical implementation is provided in Sec. II and theoretical consideration for the numerical result is given in Sec. III.

B. Information from a perturbed equilibrium

The Ideal Perturbed Equilibrium Code (IPEC) couples the DCON ideal MHD stability code with a routine for relating a specific plasma displacement $\vec{\xi}$ to a given externally produced magnetic field $\vec{b}^x$ and gives all information that can be derived from an ideal MHD equilibrium. With magnetic surfaces $\vec{x}_0(\psi, \theta, \varphi)$ in the unperturbed equilibrium, the perturbed equilibrium has surfaces $\vec{x}(\psi, \theta, \varphi) = \vec{x}_0(\psi, \theta, \varphi) + \vec{\xi}(\psi, \theta, \varphi) \cdot \hat{n}_s$, where $\hat{n}_s$ is the normal to the unperturbed magnetic surfaces.

Given the externally produced magnetic field on the plasma boundary, particular things that IPEC can calculate are: (1) The jumps in the perturbed magnetic field tangential to the magnetic surfaces, or equivalently the parallel current that is localized near the rational surfaces, which is required in ideal MHD to preserve the magnetic surfaces. (2) The magnitude of the magnetic perturbation throughout the plasma volume, $|\vec{b}|$ where $\vec{b} = \nabla \times (\vec{\xi} \times \vec{B})$, or the variation of the magnetic field strength within the magnetic surfaces.

The parallel current in the vicinity of the $q = m/n$ rational surface is measured by the jump in the perturbed magnetic field tangential to the magnetic surfaces, or equivalently [11]

$$\Delta_{mn} \equiv \left[\frac{\partial}{\partial \psi} \frac{\vec{b} \cdot \nabla \psi}{\vec{B} \cdot \nabla \varphi} \right]_{mn}, \qquad (1)$$

where only the resonant component m and n is considered in calculation of the jump $[\cdots]$. When a pressure gradient exists at the rational surface $q = m/n$, the interpretation of the jump is subtle due to the large Pfirsch-Schlüter, $j_{||}/B$, current that arises from $\vec{B} \cdot \nabla(j_{||}/B) = -(\vec{B} \times \nabla p) \cdot \nabla(1/B^2)$, near the rational surface. This phenomenon is known as the Glasser effect [12, 13]. If the Eq. (1) is interpreted as the jump across a fraction of the radial coordinate $|\delta\psi/\psi|$, then for cases we have investigated, the current given by Δ_{mn} is well behaved if one calculates the current flowing in a narrow channel but no narrower than approximately 10^{-3} of the plasma radius–a width comparable to the narrowest width at which MHD could be a valid model, the gyroradius of the ions or the electrons. If one ignores the region of validity of MHD and calculates the current flowing in narrower channels, interesting variations occur at 10^{-5} of the plasma radius.

The magnitude of Δ_{mn} for a given external magnetic field is a measure of how wide the magnetic island would be if this localized current were to dissipate. If this localized current is not dissipated, then the island does not open, but energy must come out of the plasma to the maintain the current in the presence of resistivity. In an MHD model, the flow velocity of the plasma dotted into a force between the plasma and the magnetic perturbation must balance the ηj^2 dissipation. Even when an island does not open, there can be a significant drag between

the plasma and the perturbation.

The magnitude of the magnetic perturbation, $|\vec{b}|$, in a plasma due to an external field error can be larger than one would expect from a vacuum calculation of the error penetration. This happens not only through a different inner profile of perturbed magnetic field, but also by general amplification of the external magnetic perturbation. The averaged $|\vec{b}|$ on the magnetic surfaces is a well defined quantity showing how the actual field and the vacuum penetrating field can be different inside plasma. It is related to the change in the magnetic field strength at a given spatial point,

$$|\vec{B} + \vec{b}|^2 - |\vec{B}|^2 = 2(\vec{B} \cdot \vec{b}) + |\vec{b}|^2. \qquad (2)$$

The first term $\vec{B} \cdot \vec{b}$ is usually very small, but more physical importance lies in the the variation of magnetic field strength on the perturbed flux surfaces [14], which is the Lagrangian change in the field strength. The first term in the Lagrangian change in the field strength, $(\vec{B} \cdot \vec{b})_L$, is expected to be much larger than $\vec{B} \cdot \vec{b}$ or $|\vec{b}|$, since the primary cause of this variation is generally the wobble of the magnetic surfaces rather than the variation of the magnetic field strength itself at a given spatial point. As the first computational work for the perturbed equilibria in the axisymmetric configuration, this paper provides the numerical examples of the Δ_{mn} and $|\vec{b}|$ in Sec. IV.

II. NUMERICAL IMPLEMENTATION

As discussed in the Introduction, the actual field $\vec{b} \cdot \hat{n}$ is associated with the external surface current $\vec{K}^x$ and the $\vec{K}^x$ gives the required external field $\vec{b}^x \cdot \hat{n}$ to support each of the M neighboring equilibria. Their interrelations are expressed by linear operators as $\vec{b} \cdot \hat{n} = \hat{\Lambda} \left[\vec{K}^x \right]$ and $\vec{b}^x \cdot \hat{n} = \hat{L} \left[\vec{K}^x \right]$, respectively, in the real space (θ, φ) on the unperturbed plasma boundary, or equivalently on a control surface. The actual field and the external field are finally related by $\vec{b} \cdot \hat{n} = \hat{P} \left[\vec{b}^x \cdot \hat{n} \right]$ through a linear operator $\hat{P} = \hat{\Lambda}\hat{L}^{-1}$. These linear operators can be represented as matrices and constructed to the required accuracy using a sufficiently large number M of the perturbed equilibria found by DCON. That is, with proper functional bases, one can express the functions of $\vec{b} \cdot \hat{n}$, $\vec{K}^x$ and $\vec{b}^x \cdot \hat{n}$ by flux and current vectors and the operators of $\hat{\Lambda}$, $\hat{L}$ and $\hat{P}$ by inductance and permeability matrices [11, 15]. The interfaces between an arbitrary actual field, surface current and external field are constructed in this way by IPEC.

In the implementation, the operator $\hat{L}$ is obtained by calculating the external surface current $\vec{K}^x$ from the given external field $\vec{b}^x \cdot \hat{n}$ rather than calculating the field $\vec{b}^x \cdot \hat{n}$ from the surface current $\vec{K}^x$. The set of the given external fields $\vec{b}^x_i \cdot \hat{n}$ is expanded as the set

of the actual fields $\vec{b}_i \cdot \hat{n}$ found by DCON. In this way, one can complete the problem by calculating the tangential magnetic fields for the external surface current $\mu_0 \vec{K}^x_i = \hat{n} \times \vec{b}^{(vo)}_i - \hat{n} \times \vec{b}^{(p)}_i$ to obtain $\hat{\Lambda}$ and a different surface current $\mu_0 \vec{K}^v_i = \hat{n} \times \vec{b}^{(vo)}_i - \hat{n} \times \vec{b}^{(vi)}_i$ to obtain $\hat{L}$, from the given normal field $\vec{b}_i \cdot \hat{n}$ of the M neighboring equilibria found by a single DCON run. Here the purpose of the vacuum surface current $\vec{K}^v$ is only to obtain the operator $\hat{L}$ by solving inversely the Ampere's law $\nabla \times \vec{b} = \mu_0 \vec{j}$ in vacuum. The superscripts (p), (vo) and (vi) are used for discriminating between the tangential fields of the plasma, the vacuum outside and inside the plasma boundary, respectively. To calculate them, one can introduce surface current potentials κ for the surface currents and effective magnetic scalar potentials χ for the tangential fields. The details are described in the following subsections.

A. Inductances and permeability

The normal perturbed magnetic fields of the M neighboring equilibria can be represented in the Fourier space, where M poloidal harmonics, m, construct each normal magnetic field. Since the unperturbed equilibria are axisymmetric, the toroidal harmonic numbers, n, are uncoupled so they can be treated separately. With any set of flux coordinates, (ψ, θ, φ), the normal magnetic field on the plasma boundary is expanded as

$$(\vec{b} \cdot \hat{n})(\theta, \varphi) = Re \left(\sum_m \Phi_m w(\theta) e^{i(m\theta - n\varphi)} \right), \qquad (3)$$

where the weight function $w(\theta) = 1/(\mathcal{J}(\theta)|\nabla\psi|(\theta))$ with the Jacobian $\mathcal{J}(\theta)$ is used for an orthogonal basis, by the definition of $\oint w f_m f_{m'} da = \delta_{mm'}$ on the boundary surface, with $f_m = e^{i(m\theta - n\varphi)}$. Since the weight function has inverse units of area, $\vec{\Phi}$ is a matrix vector of flux that represents $\vec{b} \cdot \hat{n}$.

The jump in the tangential field across the control surface just outside the plasma gives a surface current $\vec{j} = \vec{K}\delta(\psi - \psi_b)$. The surface current can also be expressed as

$$\vec{K} = \nabla\kappa(\theta, \varphi) \times \nabla\psi \qquad (4)$$

when $\kappa(\theta, \varphi)$ is a surface current potential. This is the general form of a surface current if the current $\vec{j}$ has no component normal to the boundary and no divergence. The potential $\kappa(\theta, \varphi)$ has units of current and can be used for representing the surface current $\vec{K}$ by

$$\kappa(\theta, \varphi) = Re \left(\sum_m \mathcal{I}_m e^{i(m\theta - n\varphi)} \right) \qquad (5)$$

with the matrix vector $\vec{\mathcal{I}}$ having units of current. Combining the actual fluxes $\vec{\Phi}_i$ and external currents $\vec{\mathcal{I}}^x_i$ of

the M neighboring equilibria, one can obtain a plasma inductance matrix $\overleftrightarrow{\Lambda}$ on the Fourier space, where the M poloidal harmonics are retained. $\overleftrightarrow{\Lambda}$ gives the relation between an actual flux and an external current by

$$\vec{\Phi} = \overleftrightarrow{\Lambda} \cdot \vec{\mathcal{I}}^x. \tag{6}$$

Similarly, the external normal magnetic perturbation $\vec{b}^x \cdot \hat{n}$ producing the surface current $\vec{K}^x$ can be expanded and related to the current by

$$\vec{\Phi}^x = \overleftrightarrow{L} \cdot \vec{\mathcal{I}}^x, \tag{7}$$

where $\overleftrightarrow{L}$ is a surface inductance matrix since it depends only on the shape of the boundary surface. As described, the IPEC uses the given set of the fluxes $\vec{\Phi}_i$ of the M neighboring equilibria and computes the associated external currents $\vec{\mathcal{I}}_i^x$ to obtain $\overleftrightarrow{\Lambda}$ from $\vec{\Phi} = \overleftrightarrow{\Lambda} \cdot \vec{\mathcal{I}}^x$ and the vacuum currents $\vec{\mathcal{I}}_i^v$ to obtain $\overleftrightarrow{L}$ from $\vec{\Phi} = \overleftrightarrow{L} \cdot \vec{\mathcal{I}}^v$.

The linear relation between an actual flux $\vec{\Phi}$ and an external flux $\vec{\Phi}^x$ can be written as

$$\vec{\Phi} = \overleftrightarrow{P} \cdot \vec{\Phi}^x \tag{8}$$

with a permeability matrix $\overleftrightarrow{P} = \overleftrightarrow{\Lambda} \cdot \overleftrightarrow{L}^{-1}$. If a magnetic field error $\vec{\Phi}^x$ is specified on the boundary, one can expand it by $\vec{\Phi}^x = \sum_{i=1}^M c_i \vec{\Phi}_i^x = \sum_{i=1}^M c_i \overleftrightarrow{P}^{-1} \cdot \vec{\Phi}_i$, or equivalently by $\vec{\Phi} = \overleftrightarrow{P} \cdot \vec{\Phi}^x = \sum_{i=1}^M c_i \vec{\Phi}_i$ to obtain the perturbed equilibrium by $\vec{\xi}(\psi, \theta, \varphi) = \sum_{i=1}^M c_i \vec{\xi}_i(\psi, \theta, \varphi)$. Each actual flux $\vec{\Phi}_i$ is associated with a plasma displacement $\vec{\xi}_i$ through Eq. (3) and $\vec{b} = \nabla \times (\vec{\xi} \times \vec{B})$.

B. Magnetic scalar potentials and surface currents

Magnetic scalar potentials are used to compute the external surface current potential κ^x and the vacuum surface current potential κ^v. When dealing with the vacuum outside and inside the plasma boundary, magnetic scalar potentials obviously exist. For the sake of clarity, we write them as

$$\nabla \chi^{(vi)} = \vec{b}^{(vi)} \tag{9a}$$
$$\nabla \chi^{(vo)} = \vec{b}^{(vo)}. \tag{9b}$$

The jump condition $\mu_0 \vec{K}^v = \hat{n} \times \vec{b}^{(vo)} - \hat{n} \times \vec{b}^{(vi)}$ gives

$$\mu_0 \kappa^v = \chi^{(vi)} - \chi^{(vo)}. \tag{10}$$

The VACUUM code [10], which is part of DCON package of codes, routinely solves $\chi^{(vo)}$ for each of the M neighboring equilibria, and the inner vacuum potential, $\chi^{(vi)}$, is related with the outer vacuum potential by

$$\frac{\chi^{(vi)}(\vec{x})}{\chi^{(vo)}(\vec{x})} = -1 + \frac{\int_c d^2\vec{x}' \hat{n} \cdot \nabla' G(\vec{x}, \vec{x}') \chi^{(vo)}(\vec{x}')}{\int_c d^2\vec{x}' \hat{n} \cdot \nabla' G(\vec{x}, \vec{x}') \chi^{(vi)}(\vec{x}')}, \tag{11}$$

where the Green function is given by $G(\vec{x}, \vec{x}') = 1/|\vec{x} - \vec{x}'|$ on the boundary.

When computing the external surface current potential κ^x, one can define a plasma magnetic scalar potential $\chi^{(p)}$ for the tangential field since a jump condition gives the relation, $\chi^{(p)} = \mu_0 \kappa^x + \chi^{(vo)}$. The necessary and sufficient conditions for the existence of the κ^x are $\vec{j} \cdot \nabla \psi = 0$ and $\nabla \cdot \vec{j} = 0$. It is trivial to prove that the perturbed equilibrium with zero-edge equilibrium pressure and current has these two properties. With non-zero edge equilibrium current, the perturbed current still can satisfy the two conditions, $\vec{j} \cdot \nabla \psi = 0$ and $\nabla \cdot \vec{j} = 0$, if one introduces an effective perturbed magnetic field $\vec{\mathfrak{B}}$ to deal with $\vec{J} \neq 0$ on the boundary.

The effective perturbed magnetic field is defined as

$$\vec{\mathfrak{B}} \equiv \vec{b} + (\vec{\xi} \cdot \hat{n})(\mu_0 \vec{J} \times \hat{n}), \tag{12}$$

which has the property $\nabla \times \vec{\mathfrak{B}} \cdot \nabla \psi = 0$ for δW minimizing perturbations, as described in the section V. C. 1 of Ref. [16]. Defining $\vec{j}$ on the control surface by

$$\vec{j} \equiv \nabla \times \vec{\mathfrak{B}}/\mu_0, \tag{13}$$

the two conditions, $\vec{j} \cdot \nabla \psi = 0$ and $\nabla \cdot \vec{j} = 0$, are satisfied. Since $\vec{\mathfrak{B}} = \vec{b}$ outside plasma, surface current or surface current potential given by $\vec{j}$ is unique for an external perturbation. The surface current can be represented by a surface current potential as in Eq. (4). Combining Eq. (13) and Eq. (4),

$$\mu_0 \nabla \kappa^x = [\vec{\mathfrak{B}}], \tag{14}$$

where [ ] denotes the jump of the quantity at the control surface, which is the tangential part of $\vec{\mathfrak{B}}$. This implies

$$\hat{n} \times \nabla \chi^{(p)} = \hat{n} \times \vec{\mathfrak{B}}^{(p)} \tag{15}$$

and the surface current potential is given by

$$\mu_0 \kappa^x = \chi^{(p)} - \chi^{(vo)}. \tag{16}$$

For the numerical examples of this paper, a zero-edge equilibrium current and pressure were used for simplicity.

Each of the described magnetic scalar potentials is expanded in the same way as the surface current,

$$\chi(\theta, \varphi) = Re\left(\sum_m \mathcal{X}_m e^{i(m\theta - n\varphi)}\right). \tag{17}$$

The magnetic scalar potential for the plasma is given by

$$\mathcal{X}_m^{(p)} = \frac{(\vec{\mathfrak{B}}^{(p)} \cdot (\partial \vec{x}/\partial \theta))_m}{im} = -\frac{(\vec{\mathfrak{B}}^{(p)} \cdot (\partial \vec{x}/\partial \varphi))_m}{in} \tag{18}$$

from Eq. (15). The equality of the two forms for $\mathcal{X}_m^{(p)}$ are checked during the computation. The magnetic scalar potential for the vacuum inside the plasma boundary is given by

$$\vec{\mathcal{X}}^{(vi)} = -(\overleftrightarrow{I} - \overleftrightarrow{K})^{-1} \cdot (\overleftrightarrow{I} + \overleftrightarrow{K}) \cdot \vec{\mathcal{X}}^{(vo)}, \tag{19}$$

where $\overleftrightarrow{I}$ is the identity matrix and the components of the kernel matrix $\overleftrightarrow{K}$ is given by

$$K_{mm'} = -\frac{1}{2\pi} \iint_{cc'} d\theta d\varphi d\theta' d\varphi' \nabla'\psi \cdot \nabla'G(\theta,\varphi;\theta',\varphi')$$
$$\times e^{i(m\theta - m'\theta')} e^{-i(m\varphi - m'\varphi')}. \tag{20}$$

This is the matrix representation of Eq. (11). The surface currents in Eq. (10) and (16) are represented in the functional space by

$$\mu_0 \vec{\mathcal{I}}_i^x = \vec{\mathcal{X}}_i^{(p)} - \vec{\mathcal{X}}_i^{(vo)} \tag{21a}$$
$$\mu_0 \vec{\mathcal{I}}_i^v = \vec{\mathcal{X}}_i^{(vi)} - \vec{\mathcal{X}}_i^{(vo)}. \tag{21b}$$

Each set of magnetic scalar potentials, $\vec{\mathcal{X}}_i^{(p)}$, $\vec{\mathcal{X}}_i^{(vo)}$ and $\vec{\mathcal{X}}_i^{(vi)}$ is used to compute the associated surface currents for the M neighboring equilibria.

III. THEORETICAL CONSIDERATIONS

The methodology described in the previous sections gives the external surface current $\vec{K}^x$ on the control surface that represents the externally produced magnetic field $\vec{b}^x$, which is specified on the boundary. Since an external perturbation comes from the externally driven current, all the perturbed energy δW should come from the external current, or equivalently the surface current $\vec{K}^x$ on the control surface. This section will show this by considering the perturbation theory of MHD.

A. Perturbed energy

The perturbed potential energy of plasma is given by

$$\delta W_{pot} = -\frac{1}{2} \int_p \vec{\xi} \cdot \vec{F}(\vec{\xi}) d^3x, \tag{22}$$

where the ideal MHD force operator $\vec{F}$ is

$$\vec{F} = \vec{J} \times \vec{b} + \vec{j} \times \vec{B} - \nabla p \tag{23}$$

in ideal MHD. The perturbed quantities are magnetic field $\vec{b}$, current $\vec{j}$ and pressure p. Assuming that equilibrium pressure P goes to zero before the plasma edge is reached, an integration by parts of the term $\vec{\xi} \cdot (\vec{j} \times \vec{B})$ allows us to write the total potential energy as [6]

$$\delta W_{pot} = \delta W_p + \int_o \frac{|\vec{b}|^2}{2\mu_0} d^3x - \int_o \frac{1}{2}\vec{j} \cdot \vec{a} d^3x, \tag{24}$$

where $\vec{a} \equiv \vec{\xi} \times \vec{B}$ is a perturbed vector potential. The integral over the plasma volume, δW_p, has various equivalent forms [17]. The subscript o on the integrals denotes an integration over the region outside the plasma.

Since the external surface current on the control surface is the only current outside the plasma, Eq. (24) can be rewritten as

$$\delta W_{pot} = \delta W_p + \int_o \frac{|\vec{b}|^2}{2\mu_0} d^3x - \int_c \frac{1}{2}\kappa^x \vec{b} \cdot d\vec{s}, \tag{25}$$

where the subscript c on the last integral denotes a surface integral on the control surface. Energy conservation implies that $\delta W_{tot} = \delta W_k + \delta W_{pot} = 0$ when δW_k is the kinetic energy associated with the perturbation. However, δW_k is negligible on the time scale of external control, so the perturbed potential energy $\delta W_{pot} = 0$, so

$$\int_c \frac{1}{2}\kappa^x \vec{b} \cdot d\vec{s} = \delta W_p + \int_o \frac{|\vec{b}|^2}{2\mu_0} d^3x. \tag{26}$$

We can see that the external surface current must supply the required energy to perturb the plasma and the vacuum, so the perturbed energy is

$$\delta W \equiv \int_c \frac{1}{2}\kappa^x \vec{b} \cdot d\vec{s}. \tag{27}$$

The perturbed energy δW can be divided into plasma and vacuum parts using each magnetic scalar potential defined in Sec. III B. Using Eq. (16), Eq. (26) can be rewritten as

$$\delta W_p = \int_c \frac{1}{2\mu_0}\chi^{(p)}\vec{b} \cdot d\vec{s} \tag{28a}$$
$$\int_o \frac{|\vec{b}|^2}{2\mu_0} d^3x = -\int_c \frac{1}{2\mu_0}\chi^{(vo)}\vec{b} \cdot d\vec{s}, \tag{28b}$$

where Eq. (28b) for vacuum part is obvious by integrating by parts, but Eq. (28a) for plasma part is an implicit result of the described energy conservation. The left hand sides of Eq. (28a) and (28b) are found using DCON and the right hand sides can be obtained using IPEC. The equations in Eq. (28) provide an important check on the accuracy of the computation.

B. Verification of accuracy

Equations in (28) can be verified for each perturbed energy of the M neighboring equilibria to a given plasma state. For the computational example, a strongly shaped stable plasma was chosen and analyzed. This particular NSTX (National Spherical Torus eXperiment) [18] equilibrium and the specifics of the analysis are explained in detail in Sec. IV.

To check Eq. (28), note that the perturbation energy associated with each DCON mode is

$$\delta W_i = \frac{1}{4}(\vec{\mathcal{I}}_i^{x\dagger} \cdot \vec{\Phi}_i + \vec{\Phi}_i^\dagger \cdot \vec{\mathcal{I}}_i^x), \tag{29}$$

which is a real quantity. Equations (28a) and (28b) are

$$\delta W_{pi} = \frac{1}{4\mu_0}(\vec{\mathcal{X}}_i^{(p)\dagger} \cdot \vec{\Phi}_i + \vec{\Phi}_i^\dagger \cdot \vec{\mathcal{X}}_i^{(p)}) \tag{30a}$$
$$\int_o \frac{|\vec{b}_i|^2}{2\mu_0} d^3x = -\frac{1}{4\mu_0}(\vec{\mathcal{X}}_i^{(vo)\dagger} \cdot \vec{\Phi}_i + \vec{\Phi}_i^\dagger \cdot \vec{\mathcal{X}}_i^{(vo)}) \tag{30b}$$
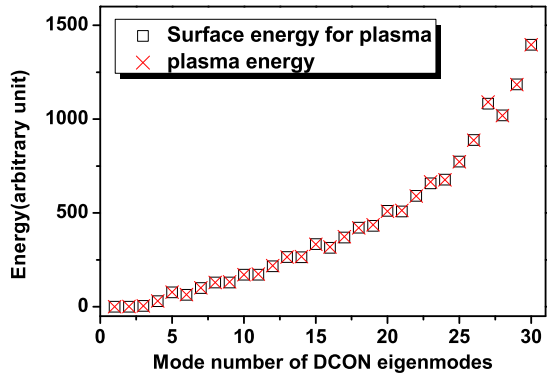
FIG. 1: (Color online) The left hand side ($\times$) of Eq. (30a) is compared with the right hand side ($\square$) for the thirty $1 \leq i \leq 30$ least stable perturbed equilibria. A given equilibrium in Fig. 4(a) is stable, so all the perturbed plasma energies should be positive.
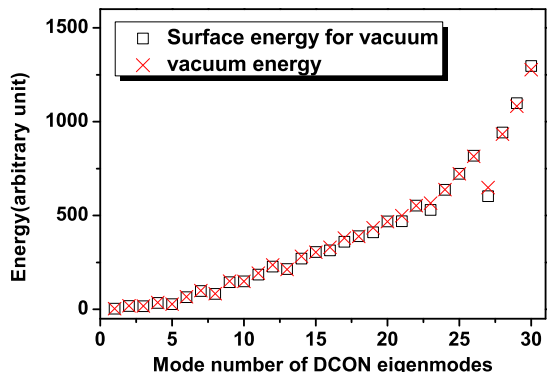

FIG. 2: (Color online) The left hand side ($\times$) of Eq. (30b) is compared with the right hand side ($\square$) for the thirty $1 \leq i \leq 30$ least stable perturbed equilibria. A given equilibrium in Fig. 4(a) is used. The perturbed vacuum energies of any equilibria should be greater than zero.

in the functional space.

Figures 1 and 2 give the energies for the left hand sides ($\times$) and the right hand sides ($\square$) of Eq. (30a) and Eq. (30b), respectively, for the first thirty modes $1 \leq i \leq 30$ of the given equilibrium.

As shown, the left and right hand sides of Eq. (30) agree and verify that the surface current carries all the perturbed energy with fairly good accuracies. Difficulties occur for the higher eigenmodes because these modes are not well represented by the fixed M poloidal harmonics retained in the DCON calculation.

Another way to check the numerical accuracy can be given by computing the effective plasma inductance $\overset{\leftrightarrow}{\Lambda}$ in two different ways. The equation (29) can be expressed
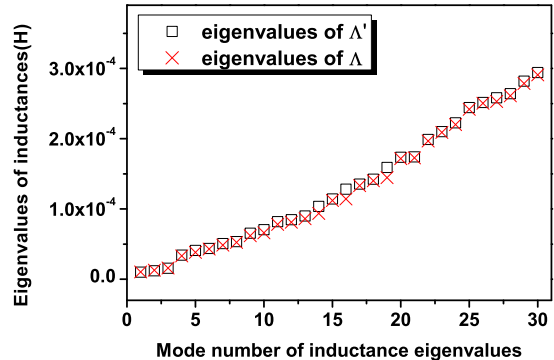
FIG. 3: (Color online) The first thirty eigenvalues of plasma inductances $\overset{\leftrightarrow}{\Lambda}$ for a given equilibrium in Fig. 4(a). Two different ways to compute the plasma inductance show a good agreement in their eigenvalues. Equations (32) and (33) are used for calculation of $\vec{\Lambda}'$ and $\overset{\leftrightarrow}{\Lambda}$, respectively.

as

$$\delta W = \frac{1}{2} \vec{\Phi}^\dagger \cdot \overset{\leftrightarrow}{\Lambda}^{-1} \cdot \vec{\Phi}, \tag{31}$$

so the $\overset{\leftrightarrow}{\Lambda}^{-1}$ can be obtained from the energy eigenvalues, without considering the perturbed surface current [19]. So we have

$$(\Lambda^{-1})_{mm'} = 2 \sum_i (\Phi^{-1})_{mi} \epsilon_i ((\Phi^{-1})^\dagger)_{im'}, \tag{32}$$

where ϵ_i is the eigenenergy value of each of the M neighboring equilibria. The $\overset{\leftrightarrow}{\Lambda}$ can also be calculated using the perturbed surface current as

$$\Lambda_{mm'} = Re(\sum_i \Phi_{mi} (\mathcal{I}^{-1})_{im'}). \tag{33}$$

Figure 3 shows good agreement of the first thirty eigenvalues of the inductance calculated by Eq. (32) and Eq. (33) and indicates that each perturbed quantity such as $\vec{\xi}, \vec{b}$ and $\vec{K}$ are computed from each other with sufficient accuracy.

IV. COMPUTATIONAL EXAMPLE

In this paper, a strongly shaped and stable plasma equilibrium of spherical torus is analyzed as an example of IPEC computation. The accuracy of the computation of the surface current and inductance for this case was verified in the previous figures 1 to 3. The NSTX configuration that was studied is shown in Fig. 4(a). It has very high $q_{edge} = 12.3$ at the normalized $\psi = 0.99$, which is taken to the boundary surface, and a strong shaping with aspect ratio $a = 1.3$, elongation $\kappa_e = 2.2$ and triangularity $\delta_{up} = 0.39, \delta_{down} = 0.43$. The plasma
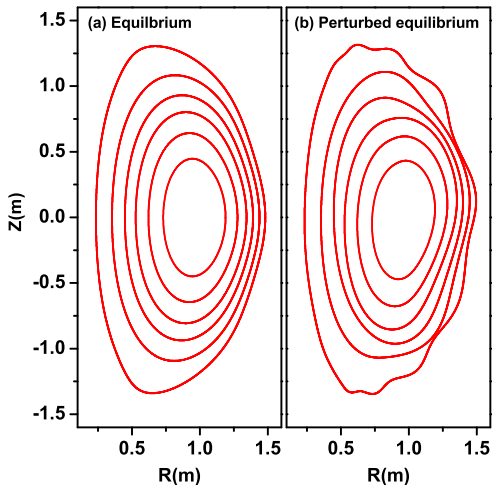
FIG. 4: (a) A given NSTX equilibrium for the computational examples in this paper. It has a strong shaping with aspect ratio $a = 1.3$, elongation $\kappa_e = 2.2$ and triangularity $\delta_{up} = 0.39$, $\delta_{down} = 0.43$ with $\beta_N = 2.0$ and $B_{T0} = 0.95T$. The boundary is taken at the normalized $\psi = 0.99$, where $q_{edge} = 12.3$. (b) A perturbed equilibrium in a toroidal section, $\varphi = 0$, for the given NSTX equilibrium with an $m = 15$ external perturbation, $\vec{b}^x \cdot \hat{n} = (15\,Gauss) \times e^{i(15\theta - \varphi)}$. The $m = 15$ external perturbation is the most amplified one among single poloidal m perturbations as explained Sec. IV A.

is stable with $\beta_N = 2.0$ and $B_{T0} = 0.95T$. The analysis is done only for $n = 1$ toroidal harmonics and by keeping $M = 41$ numbers of poloidal harmonics in the DCON calculation. Figure 4(b) shows the example of the perturbed flux surfaces for the unperturbed equilibrium in Fig. 4(a) when $m = 15$ external perturbation with $15\,G$ peak amplitude is applied on the boundary. Namely, the external perturbation on the boundary is specified by $\vec{b}^x \cdot \hat{n} = (15\,Gauss) \times e^{i(15\theta - \varphi)}$, where $15\,Gauss$ amplitude is especially used only for this example compared with $1\,Gauss$ for the rest of examples. As explained later, this $m = 15$ external perturbation is strongly amplified by the plasma, so one can see the apparent changes in the flux surfaces for this small magnetic perturbation, $|\vec{b}^x/\vec{B}| \approx 10^{-3}$. Note that the perturbed flux surfaces preserve the original magnetic topology of the unperturbed magnetic surfaces and there are no magnetic island structures in ideal MHD equations.

A. Important perturbed quantities

If one specifies an external magnetic perturbation $\vec{b}^x \cdot \hat{n}$, or equivalently $\vec{\Phi}^x$ on the boundary, the actual magnetic field or flux $\vec{\Phi}$ on the boundary can be obtained through the permeability, Eq. (8). In this section, we choose an $m = 2$ external magnetic field with $\vec{b}^x \cdot \hat{n} = (1\,Gauss) \times e^{i(2\theta - \varphi)}$ on the boundary for the computa-
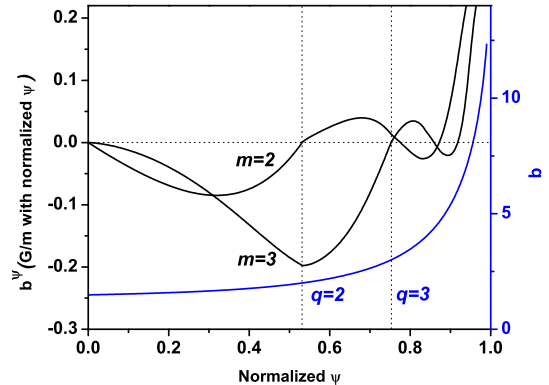

FIG. 5: The magnitude of $m = 2, 3$ contravariant normal perturbed magnetic field $\vec{b} \cdot \nabla \psi$ as a function of the normalized ψ. Only the cosine parts, $cos(2, 3\theta)cos(\varphi)$, are shown. The q profile is also provided. The each component crosses zero at the corresponding rational surface as indicated by dotted lines and has a jump of the derivative.
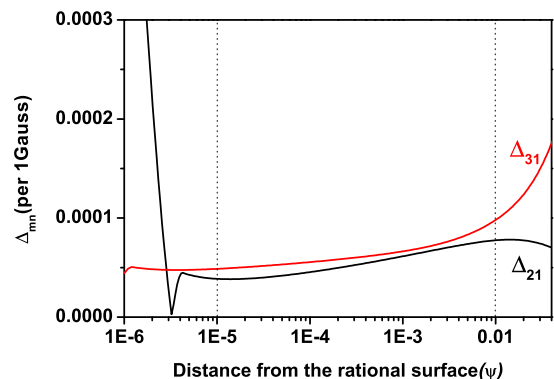

FIG. 6: The $|\Delta_{mn}|$ quantity at the $q = 2, 3$ surface as a function of the distance from each rational surface. The distance is measured by normalized ψ. The region between two dot lines has a quasi-asymtotic value of $|\Delta_{mn}|$ that has very small change down to $\psi = \pm 10^{-5}$ through a wide range of log scale.

tional examples. Since the corresponding actual field on the boundary is similar to the external perturbation as shown in Fig. 8(a), one can see the effect of plasma on inner perturbed structure with this example. Knowing the actual magnetic field on the boundary, one can obtain all the inner perturbed quantities by combining each of the M neighboring equilibria. Figure 5 shows the magnitude of $m = 2, 3$ contravariant normal perturbed magnetic field $\vec{b} \cdot \nabla \psi$ as a function of ψ. Only the cosine parts, $cos(2, 3\theta)cos(\varphi)$, are shown in the figure.

The important feature of these $(\vec{b} \cdot \nabla \psi)_{mn}$ functions is the jumps of their derivatives when they cross zero at
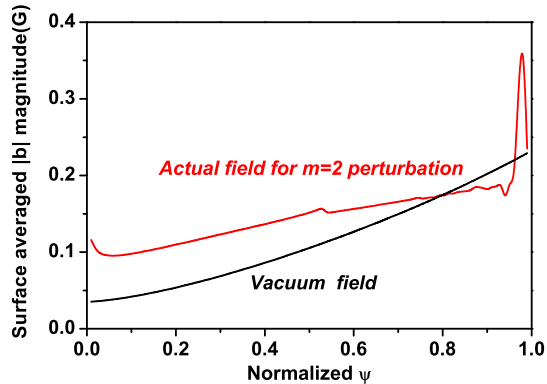
FIG. 7: (Color online) The perturbed magnetic field magnitude $|\vec{b}|$ averaged on unperturbed magnetic surfaces for the $m = 2$ external perturbation. Note that the inner profile of the actual field is apparently different from that of vacuum field even in this weakly amplifying perturbation.
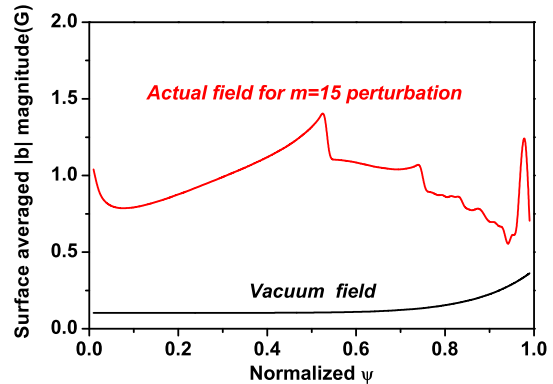

FIG. 9: (Color online) The perturbed magnetic field magnitude $|\vec{b}|$ averaged on unperturbed magnetic surfaces for the $m = 15$ external perturbation. The relative magnitude of the actual field to the vacuum field for this case is much larger than that for the $m = 2$ perturbation in Fig. 7 throughout the whole plasma.
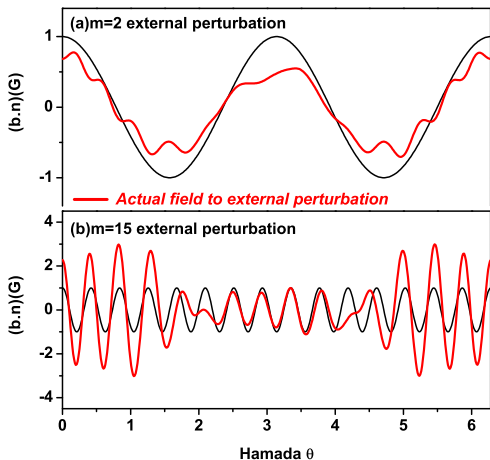
FIG. 8: (Color online) (a) The $m = 2$ external perturbation and the corresponding actual field on the boundary. The actual field is similar to the external perturbation with a small modulation. (b) The $m = 15$ external perturbation and the corresponding actual field on the boundary. General amplitude of the actual field is amplified.

their resonant surfaces. The jumps can be represented by the dimensionless quantity Δ_{mn} of Eq. (1). Δ_{mn} is proportional to the singular current required in ideal MHD to prevent an island from opening. If this singular current were dissipated, an island would open with a width proportional to $\sqrt{|\Delta|_{mn}}$.

The critical issue in the computation of Δ_{mn} is how to define the distance from the rational surface, over which Δ_{mn} is to be calculated. Ideal DCON starts to integrate the Euler-Lagrangian equation from the magnetic axis and crosses each rational surface by eliminating each

large solution component in the ideal limit. This approximation assumes the equilibrium equation $\nabla P = \vec{J} \times \vec{B}$ holds on arbitrarily small scale. Figure 6 shows $|\Delta_{21}|$ and $|\Delta_{31}|$ as a function of the half-width distance from the $q = 2$ and $q = 3$ surface, at which the jump is evaluated. As the rational surface is approached, $|\Delta_{mn}|$ has a quasi-asymptotic value that has very small change down to $\psi = \pm 10^{-5}$ through a wide range of log scale. As is illustrated in Fig. 6, the ideal approximation leads to the large changes in Δ_{mn}, and therefore the surface current, when regions around the rational surface of a few times 10^{-6} of the plasma radius are resolved. This is due to the Pfirsch-Schlüter current associated with the Glasser effect. Since MHD dose not hold on scales smaller than a gyroradius, MHD cannot be used on scales less than 10^{-2} to 10^{-3} of the plasma radius. So the strong effects of the Pfirsch-Schlüter current on the 10^{-5} to 10^{-6} scale are ignored in our analysis.

The inner profile of the $|\vec{b}|$ for the $m = 2$ external perturbation is shown in Fig. 7 . Even with this weakly amplifying perturbation, the inner profile of the actual field is different from that of the vacuum field, which is often used to approximate the perturbed magnetic field. A strongly amplified case is provided in the next section.

B. Amplification

The notion of amplification can be used for a number of perturbed quantities. Figure 8 shows the comparisons of actual field $\vec{b} \cdot \hat{n}$ for (a) $m = 2$ external perturbation with $\vec{b}^x \cdot \hat{n} = (1\,Gauss) \times Re(e^{i(2\theta - \varphi)})$ and (b) $m = 15$ external perturbation with $\vec{b}^x \cdot \hat{n} = (1\,Gauss) \times Re(e^{i(15\theta - \varphi)})$. Compared with the $m = 2$ perturbation, the actual field
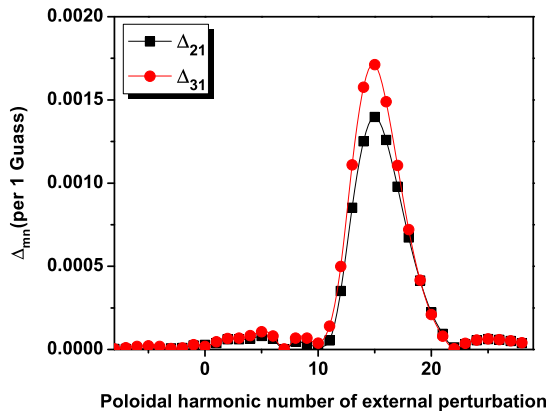
FIG. 10: (Color online) Each $|\Delta_{mn}|$ taken at the distance of normalized $\psi = \pm 10^{-3}$ from the corresponding rational surface as a function of poloidal harmonic number m of external perturbations with $\vec{b}^x \cdot \hat{n} = (1\,Gauss) \times Re(e^{i(m\theta - \varphi)})$. The $m = 15$ has the largest amplification effect and there is a broad poloidal harmonic coupling around the peak. The shift to the higher m side of the peak and a broad poloidal coupling are typical and can be seen on other magnetic surfaces and in other equilibria as well.

FIG. 11: The two singular structures of external magnetic field $\vec{b}^x \cdot \hat{n}$ on the boundary to make a large Δ_{mn}. (a) is the most singular one and (b) is the next one. Their singular eigenvalues in the SVD analysis is $d_1 = 2.17 \times 10^{-2}$ and $d_2 = 2.02 \times 10^{-3}$, respectively, so that the (a) structure should be considered as a dominant driving structure of the magnetic island opening by the factor $d_1/d_2 \sim 10$.

from the $m = 15$ perturbation is very different and has amplified amplitudes on the boundary surface. The actual $|\vec{b}|$ versus the vacuum $|\vec{b^x}|$ for the $m = 15$ external perturbation, Fig. 9, illustrates the amplified perturbed quantities inside the plasma. This strong amplification and different inner profile of perturbed magnetic field can make a large difference in several applications such as in the calculation of plasma rotation damping [20].

The amplification effect can be clearly seen in $|\Delta_{mn}|$. The half width of the inner layer is taken to be $\psi = \pm 10^{-3}$ of the plasma radius for estimating the value of $|\Delta_{21}|$ and $|\Delta_{31}|$, in order to neglect the effect of unphysical Pfirsch-Schlüter current. Figure 10 shows each $|\Delta_{mn}|$ at the corresponding rational surfaces as a function of poloidal harmonic number m of external perturbations with $\vec{b}^x \cdot \hat{n} = (1\,Gauss) \times Re(e^{i(m\theta - \varphi)})$. As shown in the figure, $m = 15$ has the largest amplification effect and there is a broad harmonic coupling around the peak. The external perturbations are specified on the boundary so that one might think that the largest amplification effect would occur when m is close to the edge resonant harmonic number, which is $m = 12$ with the $q_{edge} = 12.3$. However, the shift to the higher m side of the peak and a broad poloidal coupling are typical computational results in IPEC and can be seen on other magnetic surfaces and in other equilibria as well. This implies that the poloidal spectrum of the actual field is very different from that of the external field in a toroidal configuration, so one can not merely use the specified external field to explain physical quantities without solving the actual field in plasma. This is in contrast to cyliderical
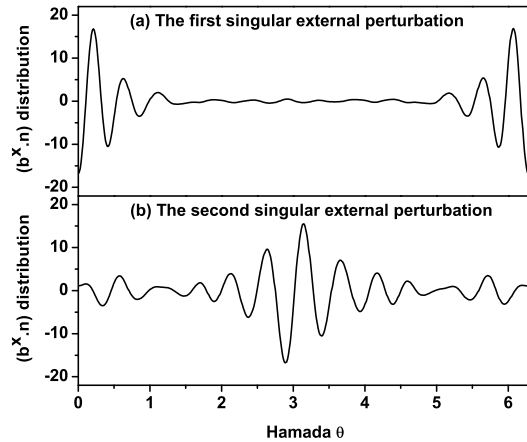
configuration, where there is no poloidal harmonic coupling.

C. Magnetic island control

The poloidal coupling spectrum in Fig. 10 can be used for controlling the opening of magnetic islands [7]. The usual error field spectrum on the boundary in many experimental devices has large amplitudes in low m numbers. Convoluting the poloidal coupling and the field spectrum will identify important m harmonic numbers to control magnetic islands. Another way to approach this problem is to create other functional bases by a SVD(Singular Value Decomposition) analysis to obtain a clear picture of the most dangerous magnetic field distribution for magnetic islands. A matrix $\mathcal{D}_{mm'}$ between the Δ_m at the resonant surfaces and the Φ_m^x on the boundary with $n = 1$ toroidal harmonic can be defined by

$$\vec{\Delta} = \overleftrightarrow{\mathcal{D}} \cdot \vec{\Phi}^x. \tag{34}$$

Considering $|\Delta_{21}|$ and $|\Delta_{31}|$ as in Fig. 10, one can find the two most singular structures on the boundary surface by using the SVD analysis for the matrix $\overleftrightarrow{\mathcal{D}}$. Figure 11 shows the two singular external field distributions $\vec{b}^x \cdot \hat{n}$. The importance of the singular distributions can be seen by comparing their singular eigenvalues $d_{1,2}$, $d_1 = 2.17 \times 10^{-2}$ and $d_2 = 2.02 \times 10^{-3}$, so that the first singular distribution is dominant by the factor $d_1/d_2 \sim 10$.

V.   SUMMARY

The IPEC has been developed for computation of three dimensional tokamak and spherical torus, based on the DCON and VACUUM codes coupled using the theory of perturbed equilibria. The ideal plasma response to external magnetic perturbation can be computed in high accuracy by the code, which constructs a relevant interface between the actual field and the external field on the control surface. The computational examples of NSTX plasma show that the actual field containing plasma response can be amplified and coupled with different poloidal harmonics. The difference between the actual field and the external field implies that one should use different components of external field from what one would expect without plasma effect, in design and control of perturbed equilibria.

[1] J. T. Scoville and R. J. LaHaye, Nucl. Fusion **43**, 250 (2003).
[2] C. G. Gimblett and R. J. Hastie, Phys. Plasmas **11**, 1019 (2004).
[3] A. Bondeson, Y. Q. Liu, D. Gregoratto, C. M. Fransson, B. Lennartson, C. Breitholtz, Y. Gribov, and V. D. Pustovitov, Phys. Plasmas **9**, 2044 (2002).
[4] S. A. Sabbagh, R. E. Bell, J. E. Menard, D. A. Gates, A. C. Sontag, J. M. Bialek, B. P. LeBlanc, F. M. Levinton, K. Tritz, and H. Yuh, Phys. Rev. Lett. **97**, 045004 (2006).
[5] M. Okabayashi, J. Bialek, M. S. Chance, M. S. Chu, E. D. Fredrickson, A. M. Garofalo, R. Hatcher, T. H. Jensen, L. C. Johnson, R. J. LaHaye, et al., Plasma Phys. Controlled Fusion **44**, B339 (2002).
[6] A. H. Boozer, Phys. Plasmas **6**, 831 (1999).
[7] C. Nührenberg and A. H. Boozer, Phys. Plasmas **10**, 2840 (2003).
[8] A. H. Boozer and C. Nührenberg, Phys. Plasmas **13**, 102501 (2006).
[9] A. H. Glasser and M. S. Chance, Bull. Am. Phys. Soc. **42**, 1848 (1997).
[10] M. S. Chance, Phys. Plasmas **4**, 2161 (1997).
[11] A. H. Boozer, Phys. Plasmas **10**, 1458 (2003).
[12] A. H. Glasser, J. M. Greene, and J. L. Johnson, Phys. Fluids **18**, 875 (1975).
[13] A. H. Glasser, J. M. Greene, and J. L. Johnson, Phys. Fluids **19**, 567 (1976).
[14] A. H. Boozer, Phys. Plasmas **13**, 044501 (2006).
[15] A. H. Boozer, Phys. Plasmas **6**, 3180 (1999).
[16] A. H. Boozer, Rev. Mod. Phys. **76**, 1071 (2004).
[17] J. P. Freidberg, *Ideal Magnetohydrodynamics* (Plenum Press , New York, 1993), pp. 241–261.
[18] J. Spitzer, M. Ono, M. Peng, D. Bashore, T. Bigelow, A. Brooks, J. Chrzanowski, H. M. Fan, P. Heitzenroeder, T. Jarboe, et al., Fusion Technology **30**, 1337 (1996).
[19] D. A. Maslovsky and A. H. Boozer, Phys. Plasmas **12**, 042108 (2005).
[20] K. C. Shaing, S. P. Hirshman, and J. D. Callen, Phys. Fluids **29**, 521 (1986).